ELSEVIER

Biophysical Chemistry 119 (2006) 23 – 32

Biophysical Chemistry

http://www.elsevier.com/locate/biophyschem

The effect of HIV-1 Gag myristoylation on membrane binding

Paxton Provitera, Raafat El-Maghrabi, S. Scarlata *

Department of Physiology and Biophysics, State University of New York at Stony Brook, Stony Brook, NY 11796-8661, USA

Received 21 June 2005; received in revised form 1 August 2005; accepted 16 August 2005
Available online 23 September 2005

Abstract

During the viral life cycle, an HIV protein, Gag, assembles at the host membrane, specifically at lipid raft regions, at very high concentrations leading to viral particle budding. Gag is post-translationally modified with an N-terminal myristate group which is thought to target Gag to lipid rafts thus aiding in assembly. Here we have analyzed the membrane binding of myristoylated HIV-1 Gag and a non-myristoylated form of HIV-1 Gag to various membrane models. After assessing the extent of myristoylation by HPLC and radiometric assays, we compared membrane binding using fluorescence methods. We found that myristoylated of Gag shows a greater than twofold increase in binding affinity to model rafts. A structural model to explain these results is presented.

Keywords: HIV-1 Gag; Myristoylation; Lipid rafts; Membrane binding; Viral assembly; Fluorescence spectroscopy

1. Introduction

The viral life cycle of human immunodeficiency virus (HIV) consists of seven distinct and vital stages; infection (viral entry), reverse transcription, insertion, protein production, assembly, viral particle budding, and maturation. Evidence exists suggesting that assembly, budding and viral entry all occur at membrane microdomains known as lipid rafts [1–7]. Lipid rafts are sphingolipid and cholesterol rich, liquid ordered clusters of saturated acyl chain lipids found within plasma membranes. The saturated acyl chains pack tighter than unsaturated chains creating phase separations between the liquid disordered and the liquid ordered phases of lipid membranes. Proteins with fatty acid modifications, such as palmitoylation and myristoylation, have been shown to be associated with lipid rafts [8].

The HIV viral envelope protein gp41, which is palmitoylated, has been shown to interact through its cytoplasmic tail with the viral structural precursor protein Gag, which is myristoylated [9,10]. The fatty acid modifications of these proteins suggest that they may be targeted to lipid rafts, and colocalization studies have supported this idea by showing lipid rafts to be the sites of assembly and budding [5,9–11]. The composition of viral particle membranes is also consistent with the importance of lipid rafts in the HIV life cycle. HIV viral particle membranes have a 2.5 fold enhancement of cholesterol, which is similar to the composition of host cell lipid rafts, and are 7.5–10.5% more ordered than host cell membranes [12,13].

In vivo mammalian cell studies have shown Gag to be sufficient for viral particle budding [14,15]. Gag is a precursor protein that is processed into four mature viral proteins; the membrane-interacting matrix (MA) protein, the core forming capsid (CA) protein, p6, whose function may involve dissociation of virions from the host, and the RNA-binding nucleocapsid (NC) protein [16]. The myristoylation site of Gag is the amino-terminal glycine which is within the MA domain. Recent mutagenesis studies involving a glycine to alanine mutant producing unmyristoylated Gag and MA proteins show reduced membrane binding affinity compared to wild type myristoylated proteins [17]. The NMR structures of myristoylated MA and myristoylated MA–CA Gag-like protein reveal sequestering of the myristyl group within a hydrophobic cavity. Interestingly, the myristoylated MA structure is very similar to unmyristoylated MA structure indicating that only minor conformational changes are required for the sequestering of the myristyl group [5].

The membrane binding abilities of myristoylated and unmyristoylated Gag and MA have been indirectly studied. In

* Corresponding author. Tel.: +1 631 444 3071; fax: +1 631 444 3432.
E-mail address: Suzanne.Scarlata@sunysb.edu (S. Scarlata).

0301-4622/$ - see front matter © 2005 Elsevier B.V. All rights reserved.
doi:10.1016/j.bpc.2005.08.008

mammalian cell lines, myristoylated versions of the proteins produce more viral particles, show protein accumulation at membranes rather than in the cytosol, and colocalize with lipid raft probes [1,2,4–7,17–19]. Previously, in vitro studies have used unmyristoylated purified viral proteins from *E. coli*. Recently, Tang et. al. produced myristoylated MA and Gag-like (residues 1–362 encompassing MA and CA) proteins by incorporating yeast N-myristyltransferase into coexpression vectors.

To quantitatively determine the difference in binding affinity between myristoylated and unmyristoylated full length Gag, coexpression vectors of human NMT and BH10 HIV-1 Gag were created and used to express the two forms in *E. coli*. Fluorescence techniques show the membrane binding affinity of myristoylated Gag to be similar to unmyristoylated Gag on model membranes except for those containing lipid rafts.

2. Materials and methods

2.1. Sample preparation

BH10 HIV-1 Gag DNA was engineered to have an N-terminal 6-his tag and was subcloned into a pet28a vector. The Gag–NMT plasmid encoded an additional T7-promoter driven human N-myristyltransferase cDNA and a ribosome binding site subcloned in tandem in pet28a. Plasmids were used to transfect BL21(DE3) *E. coli* that are engineered strains containing a copy of T7-RNA polymerase that is induced by the addition of IPTG. Cells were grown in LB medium containing kanamycin to an O.D. of 1 at 37 °C and then induced with 0.4 mM IPTG. At the time of induction, preparations with Gag–NMT and control preparations with WT Gag were supplemented with either ^{14}C labeled myristic acid (~40 μM), cold myristic acid (10 mg/L~40 μM), or a combination. Induction was at room temperature for 18–24 h. HIV-1 Gag was then purified on a nickel column (Qiagen).

2.2. Lipid vesicle preparation

Large unilamellar vesicles (LUVs, 0.1 mm diameter) composed of 100% 1-palmitoyl-2-oleoyl-sn-glycero-3-phosphatidylserine (POPS), 100% 1-palmitoyl-2-oleoyl-sn-glycero-3-phosphatidylcholine (POPC), 1:2 POPS:POPC (POPS:2POPC), 1:1:1 POPS:(2S,3R,4E)-2-acylaminooctadec-4-ene-3-hydroxy-1-Phosphocholine (Sphingomyelin):Cholesterol (POPS:SM:Ch) were prepared by extrusion. The buffer used for these studies was composed of 0.5 M NaCl, 40 mM HEPES, and 1 mM DTT unless noted otherwise.

2.3. Fluorescence titrations

Unless indicated otherwise, all fluorescence measurements were made using an ISS Fluorometer (I.S.S., Inc., Champaign, IL) with samples contained in microcuvettes with a path length of 3 mm.

Membrane binding assays using intrinsic fluorescence were conducted using 200 nM HIV-1 Gag protein and adding small amounts freshly extruded 2 mM POPS, POPS:2POPC, POPS:SM:Ch LUVs. Changes in the intrinsic fluorescence were monitored by recording the spectra using λ_{ex}=280 nm, scanning from 320–400 nm, and calculating the integrated intensity. Because binding of HIV-1 Gag protein is very strong, low concentrations of lipids could be used. The contribution of scattered light never exceeded more than 1% of the total intensity. Control studies were done to ensure that the addition of buffer alone did not affect protein fluorescence emission. Reversibility of membrane binding was carried out by binding 100 nM Gag to 10 μM POPS bilayers doped with 2% dansyl-PE (Molecular Probes, Inc.), which results in a 10% increase in dansyl emission and following the reversal of this increase when a 50-fold excess of unlabeled POPS is added. Changes are reported on the basis of changes in the emission energy whose raw values are given in the text. We analyzed the change in emission energy by first calculating the center of spectral mass (CM) for each point in the titration after subtracting for background which were identical to the samples except for the absence of protein. To monitor the shift in emission energy upon membrane binding, we normalized the emission energy (Norm EE):

$$\text{Norm EE} = (\text{CM}_\text{i} - \text{CM}_\text{x})/(\text{CM}_\text{i} - \text{CM}_\text{f})$$

where the subscripts i, x, and f denote the initial, intermediate, and final concentrations of HIV-1 Gag. CM is the center of the spectral mass in units of energy given in kilokaisers (kK), where 1 kK=1000 cm^{-1}. The percent change of this value (i.e. NormEE*100) is presented.

2.4. Data analysis

Experiments consisted of 3–21 trials with 10–14 titrations per trial. Trials were averaged point by point and then normalized individually. To obtain the apparent membrane

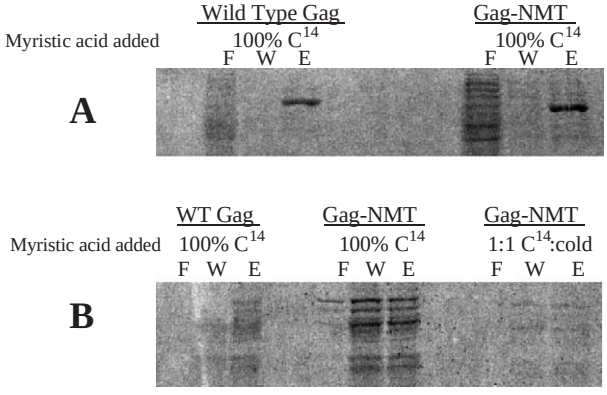

Fig. 1. Autoradiograph of ^{14}C labeled myristic acid supplemented HIV-1 Gag. A) BH10 HIV-1 Gag in pet28a vector transfected into *E. coli* and supplemented with ^{14}C labeled myristic acid during protein induction. Wild type (WT) refers to plasmid containing only Gag, whereas Gag–NMT contains both Gag and human N-myristyl transferase. F, flow through; W, wash; E, elution. B) Another example of ^{14}C myristic acid incorporation. During inoculation Gag–NMT had 100% ^{14}C myristic acid or 1:1 ^{14}C myristic acid:unlabeled myristic acid.

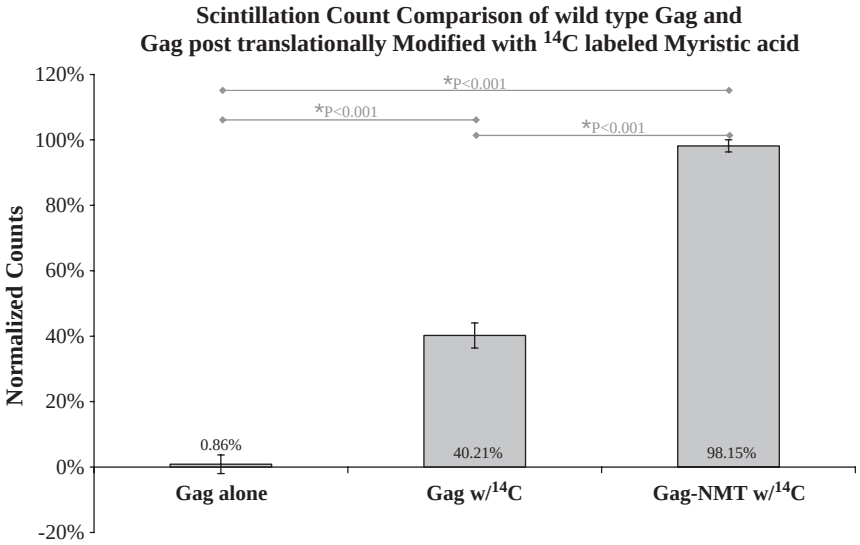

Fig. 2. Scintillation counts of ^{14}C labeled myristic acid supplemented HIV-1 Gag. HIV-1 Gag, supplemented with ^{14}C labeled myristic acid (Gag with ^{14}C) or with cold myristic acid (Gag), and HIV-1 Gag–NMT, supplemented with ^{14}C labeled myristic acid (Myr with ^{14}C), were counted on the Beckman LS 6500 Multi-purpose Counter for ^{14}C radioactivity. The results were averaged and normalized to the Myr counts with Gag at 0.86%, Gag with ^{14}C at 40.21% and Myr with ^{14}C at 98.15%.

dissociation constant (K_d) for Gag-membrane interactions, we monitored changes in the emission energy described above. We note that the term "K_d" corresponds to the apparent dissociation constant assuming that Gag partitions on membranes through nonspecific, electrostatic interactions rather than forming a chemical complex which a specific lipid(s), and no stoichiometry is inferred. K_d is defined as lipid concentration at which 50% of the protein is bound and was determined by plotting the shift in the normalized emission energy (see above) with increasing amounts of added lipid. Each titration curve, as well as the average ($n=3-15$), was fit to a hyperbola using SigmaPlot (Jandel Inc.) to obtain the apparent dissociation constant. The averaged data points, the averaged K_d, and the fitted hyperbola are graphed. Reported errors are standard error of the mean (standard deviation divided by the square root of the number of trials). Statistical analysis, using SigmaStat (Jandel Inc.), was performed for comparison of two data sets using a Student's *t*-test, and for multiple data sets using one way ANOVA and the Holm–Sidak method.

2.5. Scintillation counting

Purified protein samples from six preparations with ^{14}C labeled myristic acid were incubated with scintillation fluid and were then counted on a Beckman LS 6500 Multi-purpose

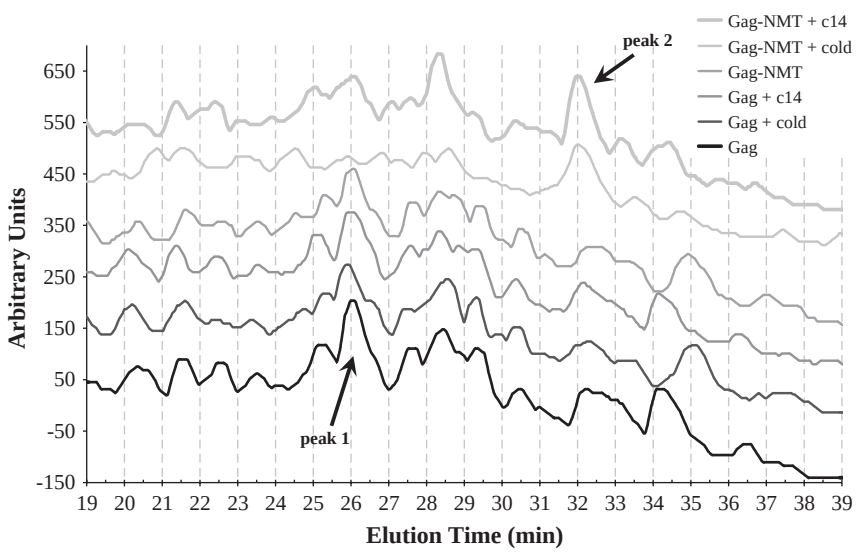

Fig. 3. Hydrophobic peptide peak shift of myristoylated Gag versus unmyristoylated Gag. Unmyristoylated (Gag) and myristoylated (Gag–NMT) were grown and supplemented with ^{14}C labeled (+c14), unlabeled (+cold) myristic acid, or no myristic acid. Purified proteins were digested using chymotrypsin and the resulting peptides were applied to a reverse phase hydrophobic HPLC column. The labeled peaks represent the hydrophobic shift of the myristoylated Gag peptides due to the increase hydrophobicity of the myristic acid modification.

Counter. Data were corrected for background, normalized to the highest value, and plotted.

2.6. Protein digestion and High Performance Liquid Chromatography (HPLC) analysis

Trichloroacetic acid (TCA) precipitation of purified Gag proteins was done by adding 100 μl of 100% TCA to 300 μl of sample to a final concentration of 20% TCA. The mixture was incubated on ice for 30 min then microfuged for 30 min at 4 °C. The pellet was then dissolved in 100 μl of 8 M urea and stored at 4 °C overnight to fully solubilize the denatured the protein. The mixture was diluted to 2 M urea by adding 300 ml of chymotrypsin digestion buffer (100 mM Tris, 100 mM NaCl and 10 mM CaCl2), and digestion was accomplished by the addition of 2 μg of chymotrypsin and overnight incubation at 37 °C.

Samples were applied to a C-18 reverse phase column on a Beckman HPLC and subjected to an elution gradient of 3 min of 95% 0.1% trifluoroacetic acid (TFA), 5% acetonitrile; 30 min of a linear gradient bringing the concentrations to 50% 0.1% TFA, 50% acetonitrile; 5 min of 50% 0.1% TFA, 50% acetonitrile; 5 min of a linear gradient bringing the concentration of acetonitrile to 100%; a 5 min wash at 100% acetonitrile followed by a 1 min linear gradient bringing the concentrations to 95% 0.1% TFA, 5% acetonitrile. Fractions of 1 ml/min were collected starting at 3 min for 40 fractions with detection at 216 nm using BioChrome Lite software.

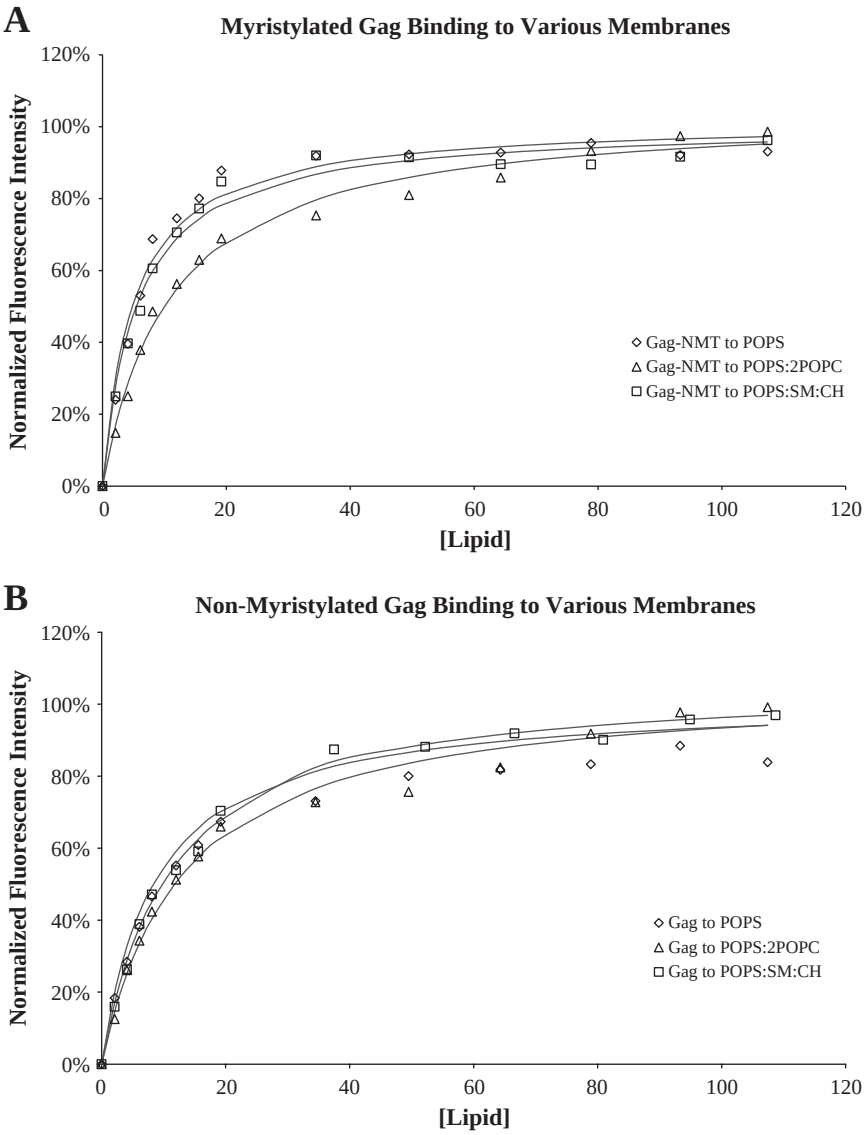

Fig. 4. Lipid binding curves of myristoylated and non-myristoylated HIV-1 Gag to various lipid membranes. A) Myristoylated Gag (Gag–NMT) to lipid binding curves for (◇) POPS (K_d=5.05±0.31 μM); (Δ) POPS:2POPC (K_d=12.22±2.13 μM); (□) POPS:SM:Ch (K_d=6.14±0.74 μM) where the initial center of spectral mass was 342 nm and underwent a 29%, 32% and 24% shift to lower wavelengths upon the addition of POPS, POPS:2POPC and POPS:SM:Ch, respectively. B) Non-myristoylated Gag (Gag) to lipid binding curves for (◇) POPS (K_d=6.51±0.56 μM); (Δ) POPS:2POPC (K_d=13.20±0.69 μM); (□) POPS:SM:Ch (K_p=11.33±1.87 μM) where the initial center of spectral mass was 340 nm and underwent a 33%, 23% and 21% shift to lower wavelengths upon the addition of POPS, POPS:2POPC and POPS:SM:Ch, respectively.

3. Results

3.1. Verification of myristoylation

To determine the role of myristoylation on Gag-membrane interactions, we transfected *E. coli* cells with plasmids containing only Gag or plasmids containing Gag and N-myristyl transferase (Gag–NMT), and grown in the presence of ^{14}C myristic acid (see Materials and methods). Gag was purified from the two preparations and samples from flow through, wash and elution stages of purification were loaded onto SDS-PAGE gels and stained with coomassie blue. Gels were then dried onto filter paper and stored with X-ray film in the freezer for 3 to 14 days with these results being shown in Fig. 1. Purified Gag–NMT incubated with ^{14}C labeled myristic acid consistently showed higher radioactivity than Gag incubated with ^{14}C labeled myristic acid or Gag–NMT incubated with a 1:1 ratio of ^{14}C labeled myristic acid and unlabeled myristic acid suggesting that Gag–NMT has a higher degree of myristoylation.

The purified samples were further analyzed for radioactivity by scintillation counting using a Beckman LS 6500 Multi-purpose Counter. This analysis corroborated the gel data by showing the radioactivity of Gag incubated with no myristic acid at 0.86% and Gag incubated with ^{14}C labeled myristic acid at 40.21% when normalized to Gag–NMT incubated with ^{14}C labeled myristic acid (Fig. 2). The percentage of Gag that is estimated to be myristoylated is within 50–90% for Gag–NMT and 20–40% for Gag.

Further verification of myristoylation was performed by growing the Gag and Gag–NMT transfected bacteria and supplementing with ^{14}C myristic acid, cold myristic acid, or unsupplemented during induction. The six samples were purified, chymotrypsin digested, and the resulting peptides were separated through a reverse phase hydrophobic HPLC column. Elution fractions 11 through 40 were analyzed for radioactivity by scintillation counting as described in Materials and methods. Low levels of radioactivity were recorded in all fractions with the highest levels, approximately three times background, in fractions 23, 24 and 30 (data not shown). Eluted peptides were monitored at 216 nm and overlaid to determine shifts in hydrophobicity of the peaks (Fig. 3). It was speculated that the primary unmyristoylated Gag control without supplementation would show a baseline unmyristoylated Gag profile because *E. coli* is devoid of N-myristyl transferase. Unmyristoylated Gag supplemented with either ^{14}C labeled or unlabeled myristic acid and myristoylated Gag without supplementation show the same baseline profile with peak 1 being sharper and more pronounced. Myristoylated Gag with supplementation of either ^{14}C labeled or unlabeled myristic acid show a reduction in peak 1 and a sharper more pronounced peak 2 suggesting a hydrophobic shift in the myristoylated Gag peptide. These studies correlate well with the observation that bacterially expressed Gag has a low level of myristylation while inclusion of N-myristyl transferase increases the amount of myristylated protein.

3.2. Membrane binding

We have previously quantified the binding of Gag to large unilamellar vesicles in terms of membrane composition, protein crowding and aggregation of membrane-bound protein [17,20]. We found that Gag binds to membranes with a strong electrostatic component due to the basic residues in MA and note that the plasma membrane contains ~30% negatively charged lipids. We measured the binding of purified Gag and Gag–NMT to electrically negative (POPS), anionic (POPS:2POPC), and membranes containing lipid rafts (PS:SM:Ch) [21] using intrinsic fluorescence as described in Materials and methods. We note that the ionic strength must be relatively high to avoid spontaneous aggregation of Gag in solution. Both proteins bound to all the membranes that were examined (Fig. 4). Comparisons of

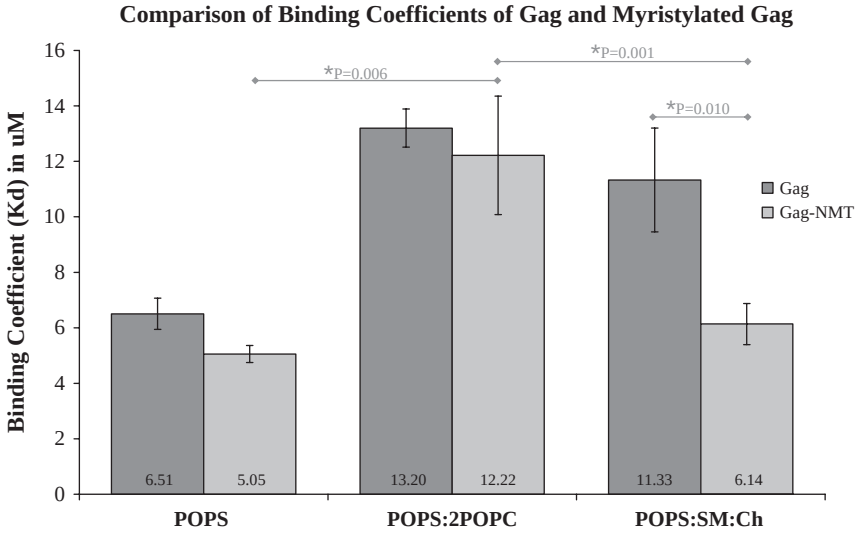

Fig. 5. Dissociation coefficient comparison of myristoylated and non-myristoylated HIV-1 Gag over various lipid membranes. 100% POPS binding coefficients for Gag (K_d=6.51±0.56 μM) and Gag–NMT (K_d=5.05±0.31 μM); POPS:2POPC binding coefficients for Gag (K_p=13.20±0.69 μM) and Gag–NMT (K_d=12.22±2.13 μM); POPS:SM:Ch binding coefficients for Gag (K_p=11.33±1.87 μM) and Gag–NMT (K_p=6.14±0.74 μM).

Gag and Gag–NMT binding coefficients showed no significant difference when bound to 100% POPS membranes (Gag $K_d = 6.51 \pm 0.56$ μM; Gag–NMT $K_d = 5.05 \pm 0.31$ μM) or POPS:2POPC membranes (Gag $K_d = 13.20 \pm 0.69$ μM; Gag–NMT $K_d = 12.22 \pm 2.13$ μM). Conversely, the lipid raft model membrane of POPS:SM:Ch revealed a significant difference between the two proteins (Gag $K_d = 11.33 \pm 1.87$ μM; Gag–NMT $K_d = 6.14 \pm 0.74$ μM), with the myristoylated Gag showing twofold greater affinity (Fig. 5).

4. Discussion

Within cellular plasma membranes, subdomains of highly concentrated sphingomyelin and cholesterol exist in the liquid ordered phase. These subdomains, known as lipid rafts, act as stable refuges within the generally liquid disordered phased membrane. Lipid rafts have been implicated in cellular signaling, endocytosis, exocytosis, viral infection, and viral budding. Lipid rafts act as clustering centers for lipid modified proteins on both the inner and outer leaflets. Myristoylation and palmitoylation are examples of modifications that assist in protein association with lipid rafts.

The viral precursor protein, Gag, is myristoylated at the N-terminal glycine which is within the membrane binding region of the MA domain. MA has been shown to interact with the cytoplasmic tail of gp41, the transmembrane viral envelope protein [10,22]. The envelope protein gp41 is in turn palmitoylated twice and as such is associated with lipid rafts.

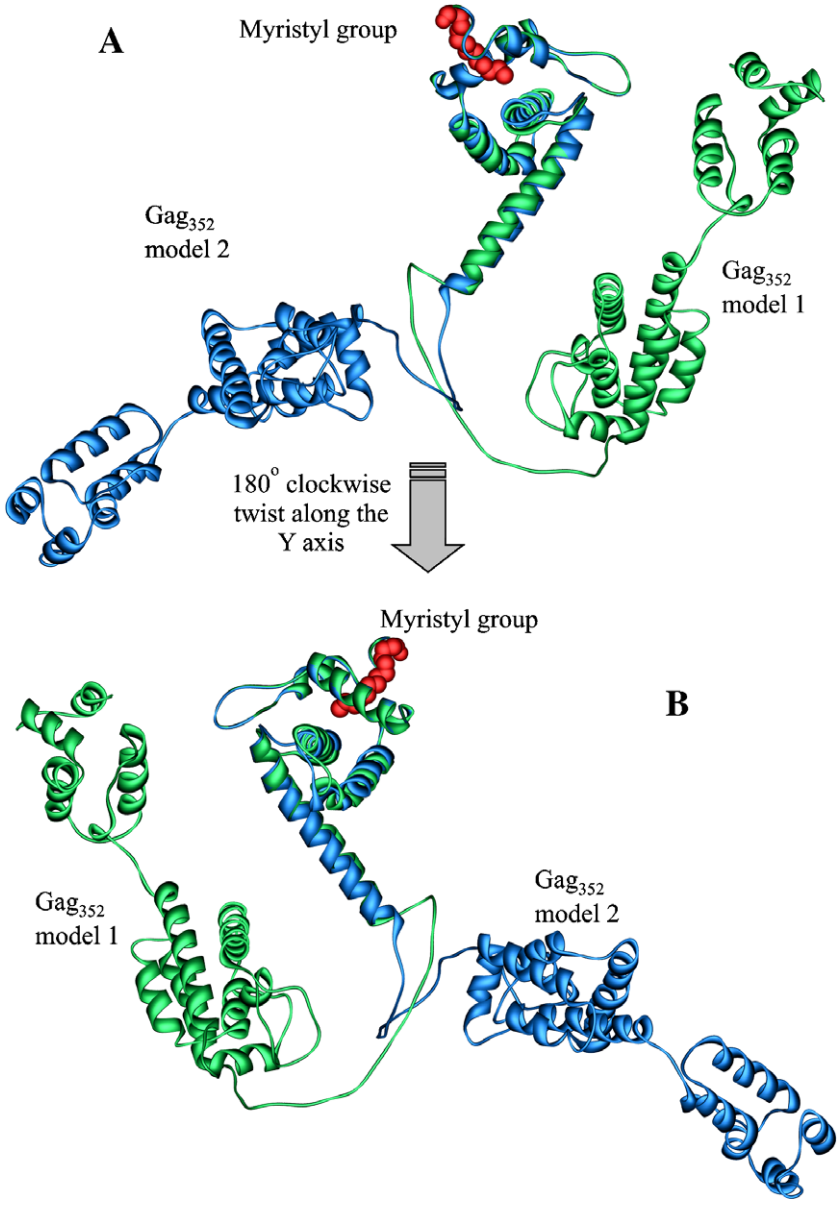

Fig. 6. Structural models of the first 352 amino-terminal residues of Gag. Models are carboxyl-terminal extensions of the myristoylated MA NMR structure [19] using the Tang 283 residue Gag NMR structure [23] and the CA crystal structure [24] with model 1 in green and model 2 in blue. The myristic acid of each model is shown in red CPK representation. The models are aligned at the MA domain. A) Side view with the membrane binding region of MA at the top center. B) 180° rotation of A. (For interpretation of the references to colour in this figure legend, the reader is referred to the web version of this article.)

Gag is capable of forming enveloped immature viral particles in the absence of other viral proteins. However, without myristoylation, Gag loses this ability although it forms spherical aggregates within the cytosol [14,15,17,18,23]. Therefore, myristoylation appears to be vital for membrane binding, assembly at membrane, and viral particle budding.

Cotranslational modification of Gag by covalent linkage of the saturated fatty acid, myristic acid, to the amino-terminal glycine is mediated by the enzyme N-myristyltransferase (NMT). This enzyme is common within mammalian cells, but is absent in *E. coli*. In order to produce large amounts of purified protein, human NMT cDNA was inserted into bacterial expression vectors containing 6-His tagged BH10 HIV-1 Gag (Gag–NMT). Analysis of ^{14}C radioactivity within these proteins produced by this expression vector revealed approximately 50% to 90% myristoylation; double that of the expression vector without an NMT (Gag). In support of these results, radioactivity counts for the Gag plasmid supplemented with ^{14}C labeled myristic acid were 40.21% compared to 98.15% for supplemented Gag–NMT and 0.86% for Gag without supplementation (Fig. 2). Although the radioactivity level of Gag is substantially lower than Gag–NMT, it was expected to be closer to background (Gag without supplementation) levels. It is possible that, with freely available myristic

Fig. 7. Structural model 1 of a myristoylated form of the first 352 amino-terminal residues of Gag in trimer form. Model 1 of Fig. 6 was aligned to the crystal structure of MA. Gag monomer subunits are shown in pink, orange and green with their myristyl groups shown in shades of red. A) Side view of myristoylated Gag trimer with the membrane binding region of MA at the top center. B) Top view of myristoylated Gag trimer (as seen from the membrane). (For interpretation of the references to colour in this figure legend, the reader is referred to the web version of this article.)

acid, there is a basal level of bacterially catalyzed amino-terminal myristoylation that becomes pronounced during the long term induction of 18–24 h.

Another reason for the high level of ^{14}C-Gag seen in the absence of NMT is that the bacteria use the supplemented myristic acid as an amino acid precursor and incorporate the radioactive carbon atoms elsewhere within the produced proteins. This second possibility could explain the low level of radioactivity seen throughout all the HPLC fractions; however, this does not detract from the consistently higher Gag–NMT radioactivity observed and the possibility of veritable N-myristoylation. Hydrophobicity peak shifts (Fig. 3) indicate the ability of Gag–NMT to increase the hydrophobicity of the protein. Short, broad peaks at the specified peak 2 within all Gag vectors and Gag–NMT without supplementation as compared to the tall sharp peaks of Gag–NMT with supplementation, indicate lower levels of myristoylation in cells without NMT or with NMT, but without supplementation. Additionally, the opposite trend within specified peak 1 indicates lower levels of unmyristoylated Gag in cells with NMT. Minor variations in

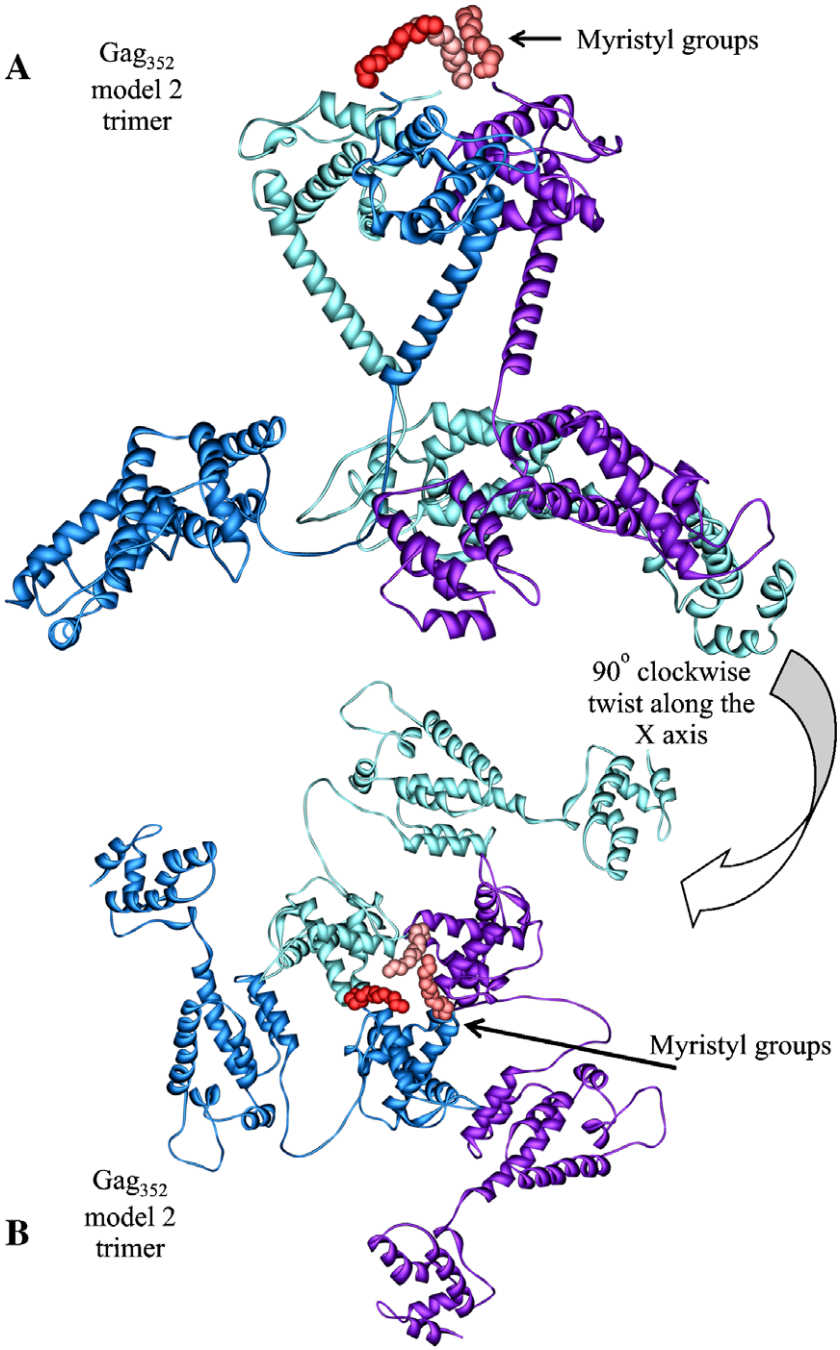

Fig. 8. Structural model 2 of a myristoylated form of the first 352 amino-terminal residues of Gag in trimer form. Model 2 of Fig. 6 was aligned to the crystal structure of MA. Gag monomer subunits are shown in cyan, purple and blue with their myristyl groups shown in shades of red. A) Side view of myristoylated Gag trimer with the membrane binding region of MA at the top center. B) Top view of myristoylated Gag trimer (as seen from the membrane). (For interpretation of the references to colour in this figure legend, the reader is referred to the web version of this article.)

peak height correspond to slight differences in protein production and can be neglected. These multiple lines of evidence provide confirmation that larger amounts of myristoylated Gag are produced by cells transfected with Gag–NMT.

The NMR structure of myristoylated MA (myr-MA) has been solved in the monomer form [19] and is in close agreement with the unmyristoylated MA structure [24]. The myristyl group penetrates ~10 Å beneath the surface of the protein but maintains an extended conformation that leaves ~40% exposed to solvent. Although the myristyl group is sequestered in the monomeric form, there is evidence of a concentration dependent myristate exposed trimer. The myr-MA trimer shows similarities to the unmyristoylated MA trimer [24], suggesting trimer assembly may be promoted by intermolecular myristic acid interactions. This interaction can be accommodated in models without disrupting the tertiary structure of the monomer. A myristoylated Gag-like construct of residues 1–362 (myr-MA–CA) was created and investigated via NMR techniques. Even though the NMR structures of both the monomer and trimer forms of myr-MA–CA were unresolved, observed NMR signals followed the same trends as seen with myr-MA and the previously determined NMR structure of the amino-terminal 283 residues of Gag which was unmyristoylated [25]. Two possible structural models of myristoylated Gag monomer were created by alignment of myr-MA NMR structures with models 1 and 2 of the 20 submitted NMR structures of the amino-terminal 283 residues of Gag (Fig. 6). The two models correspond to two conformations of the linker region of Gag that connects MA to CA. Model 1 is representative of the best conformer in the NMR structure of the amino-terminal 283 residues of Gag, however this model brings the CA domain into close proximity of a theoretical membrane and deviates from the commonly proposed elongated, cylindrical structure of Gag. Model 2 more closely resembles an elongated version of Gag. Models of the myristoylated Gag trimer based on the NMR and sedimentation equilibrium data [19], constructed from the NMR structure of the N-terminal 283 residues [25] of Gag and the crystal structure of CA [26], and aligned with the MA trimer crystal structure [24] show fully exposed myristyl groups that can embed themselves within lipid rafts (Figs. 7 and 8).

Myristoylated Gag would be expected to preferentially bind lipid rafts over liquid disordered phase plasma membranes. Determination of this preferential binding was carried out by monitoring intrinsic fluorescence while increasing the concentration of the model membrane. Myristoylated Gag (Gag–NMT) showed a twofold increase in binding affinity over unmyristoylated Gag (Gag). Considering that our comparison was made between Gags that were on average 20–40% and 50–90% myristoylated, the differences in binding due to myristoylation may be significant. The additional binding energy associated with a myristic acid modification to a protein is on the order of 10^{-4} M [27]. This slight increase in binding affinity could account for the observed twofold increase, on the order of 10^{-6} M, of Gag–NMT binding only in multimeric form with full exposure of the myristyl group as seen in the trimeric structural models (Figs. 7 and 8). Work is currently underway to solve the structure of full length Gag in both the myristoylated and unmyristoylated forms. Once those structures are resolved, further insight into the role of myristoylation can be ascertained.

References

[1] W. Popik, T.M. Alce, W.C. Au, Human immunodeficiency virus type 1 uses lipid raft-colocalized CD4 and chemokine receptors for productive entry into CD4(+) T cells, J. Virol. 76 (10) (2002) 4709–4722.

[2] S. Nisole, B. Krust, A.G. Hovanessian, Anchorage of HIV on permissive cells leads to coaggregation of viral particles with surface nucleolin at membrane raft microdomains, Exp. Cell Res. 276 (2) (2002) 155–173.

[3] D.H. Nguyen, D. Taub, CXCR4 function requires membrane cholesterol: implications for HIV infection, J. Immunol. 168 (8) (2002) 4121–4126.

[4] S.M. Campbell, S.M. Crowe, J. Mak, Lipid rafts and HIV-1: from viral entry to assembly of progeny virions, J. Clin. Virol. 22 (3) (2001) 217–227.

[5] D.H. Nguyen, J.E. Hildreth, Evidence for budding of human immunodeficiency virus type 1 selectively from glycolipid-enriched membrane lipid rafts, J. Virol. 74 (7) (2000) 3264–3272.

[6] K. Holm, et al., Human immunodeficiency virus type 1 assembly and lipid rafts: Pr55(gag) associates with membrane domains that are largely resistant to brij98 but sensitive to triton X-100, J. Virol. 77 (8) (2003) 4805–4817.

[7] L. Ding, et al., Independent segregation of human immunodeficiency virus type 1 Gag protein complexes and lipid rafts, J. Virol. 77 (3) (2003) 1916–1926.

[8] M.D. Resh, Membrane targeting of lipid modified signal transduction proteins, Subcell. Biochem. 37 (2004) 217–232.

[9] D.J. Wyma, et al., Coupling of human immunodeficiency virus type 1 fusion to virion maturation: a novel role of the gp41 cytoplasmic tail, J. Virol. 78 (7) (2004) 3429–3435.

[10] X. Yu, The matrix protein of human immunodeficiency virus type 1 is required for incorporation of viral envelope protein into mature virions, J. Virol. 66 (8) (1992) 4966–4971.

[11] B.G. Turner, M.F. Summers, Structural biology of HIV, J. Mol. Biol. 285 (1) (1999) 1–32.

[12] R.C. Aloia, H. Tian, F.C. Jensen, Lipid composition and fluidity of the human immunodeficiency virus envelope and host cell plasma membranes, Proc. Natl. Acad. Sci. U. S. A. 90 (11) (1993) 5181–5185.

[13] R.C. Aloia, et al., Lipid composition and fluidity of the human immunodeficiency virus, Proc. Natl. Acad. Sci. U. S. A. 85 (3) (1988) 900–904.

[14] D. Gheysen, et al., Assembly and release of HIV-1 precursor Pr55gag virus-like particles from recombinant baculovirus-infected insect cells, Cell 59 (1) (1989) 103–112.

[15] E. Jacobs, et al., The HIV-1 Gag precursor Pr55gag synthesized in yeast is myristoylated and targeted to the plasma membrane, Gene 79 (1) (1989) 71–81.

[16] J.M. Coffin, S.H. Hughes, H. Varmus, Retroviruses, Cold Spring Harbor Laboratory Press, Plainview, N.Y., 1997, xv, 843 pp.

[17] F. Bouamr, S. Scarlata, C. Carter, Role of myristylation in HIV-1 Gag assembly, Biochemistry 42 (21) (2003) 6408–6417.

[18] M. Bryant, L. Ratner, Myristoylation-dependent replication and assembly of human immunodeficiency virus 1, Proc. Natl. Acad. Sci. U. S. A. 87 (2) (1990) 523–527.

[19] C. Tang, et al., Entropic switch regulates myristate exposure in the HIV-1 matrix protein, Proc. Natl. Acad. Sci. U. S. A. 101 (2) (2004) 517–522.

[20] P. Provitera, et al., Role of the major homology region in assembly of HIV-1 Gag, Biochemistry 40 (18) (2001) 5565–5572.

[21] S. Scarlata, Regulation of the lateral association of phospholipase Cbeta2 and G protein subunits by lipid rafts, Biochemistry 41 (22) (2002) 7092–7099.

[22] H.R. Gelderblom, M. Ozel, G. Pauli, Morphogenesis and morphology of HIV. Structure–function relations, Arch. Virol. 106 (1–2) (1989) 1–13.

[23] R. Pal, et al., Myristoylation of gag proteins of HIV-1 plays an important role in virus assembly, AIDS Res. Hum. Retrovir. 6 (6) (1990) 721–730.

[24] C.P. Hill, et al., Crystal structures of the trimeric human immunodeficiency virus type 1 matrix protein: implications for membrane association and assembly, Proc. Natl. Acad. Sci. U. S. A. 93 (7) (1996) 3099–3104.
[25] C. Tang, Y. Ndassa, M.F. Summers, Structure of the N-terminal 283-residue fragment of the immature HIV-1 Gag polyprotein, Nat. Struct. Biol. 9 (7) (2002) 537–543.
[26] C. Berthet-Colominas, et al., Head-to-tail dimers and interdomain flexibility revealed by the crystal structure of HIV-1 capsid protein (p24) complexed with a monoclonal antibody Fab, Embo J. 18 (5) (1999) 1124–1136.
[27] R.M. Peitzsch, S. McLaughlin, Binding of acylated peptides and fatty acids to phospholipid vesicles: pertinence to myristoylated proteins, Biochemistry 32 (39) (1993) 10436–10443.